Int J Legal Med (2015) 129:1127–1136
DOI 10.1007/s00414-015-1218-y

ORIGINAL ARTICLE

Postmortem quantitative 1.5-T MRI for the differentiation and characterization of serous fluids, blood, CSF, and putrefied CSF

Wolf-Dieter Zech[1] · **Nicole Schwendener**[1] · **Anders Persson**[2] · **Marcel J. Warntjes**[2] · **Fabiano Riva**[1] · **Frederick Schuster**[1,3] · **Christian Jackowski**[1]

Received: 20 October 2014 / Accepted: 22 June 2015 / Published online: 11 July 2015

Abstract The purpose of the present study was to investigate whether serous fluids, blood, cerebrospinal fluid (CSF), and putrefied CSF can be characterized and differentiated in synthetically calculated magnetic resonance (MR) images based on their quantitative T_1, T_2, and proton density (PD) values. Images from 55 postmortem short axis cardiac and 31 axial brain 1.5-T MR examinations were quantified using a quantification sequence. Serous fluids, fluid blood, sedimented blood, blood clots, CSF, and putrefied CSF were analyzed for their mean T_1, T_2, and PD values. Body core temperature was measured during the MRI scans. The fluid-specific quantitative values were related to the body core temperature. Equations to correct for temperature differences were generated. In a 3D plot as well as in statistical analysis, the quantitative T_1, T_2 and PD values of serous fluids, fluid blood, sedimented blood, blood clots, CSF, and putrefied CSF could be well differentiated from each other. The quantitative T_1 and T_2 values were temperature-dependent. Correction of quantitative values to a temperature of 37 °C resulted in significantly better discrimination between all investigated fluid mediums. We conclude that postmortem 1.5-T MR quantification is feasible to discriminate between blood, serous fluids, CSF, and putrefied CSF. This finding provides a basis for the computer-aided diagnosis and detection of fluids and hemorrhages.

Keywords Postmortem quantitative MRI · Forensic imaging · Serous fluids · Blood · Putrefaction

Abbreviations

AUC	Area under curve
CSF	Cerebrospinal fluid
MRI	Magnetic resonance imaging
PMMRI	Postmortem magnetic resonance imaging
PMI	Postmortem interval
RAI	Radiological alteration index
ROC	Receiver operating characteristic
ROI	Region of interest
T	Tesla
T_2w	T_2-weighted
T_1w	T_1-weighted
PD	Proton density
TI	Inversion time
TR	Repetition time
TE	Echo time

Introduction

Postmortem magnetic resonance imaging (PMMRI) has become a useful adjunct tool to forensic autopsy [1–5]. In addition to its recognized role in the depiction of soft tissue and internal organs, MRI is effective in detecting fluid mediums when the appropriate MRI sequences are used [6–8]. The identification of the nature of the detected fluid medium is highly relevant because it can be an indication of trauma or pathologic processes [9–15]. In conventional MR images, fluid mediums are

✉ Wolf-Dieter Zech
wolf-dieter.zech@irm.unibe.ch

1 Institute of Forensic Medicine, University of Bern, Bühlstrasse 20, 3012 Bern, Switzerland

2 Center for Medical Image Science and Visualization (CMIV), Linköping University, Linköping, Sweden

3 Department of Diagnostic, Interventional and Pediatric Radiology, Hospital and University of Bern Inselspital, Freiburgstrasse 10, 3010 Bern, Switzerland

recognized by their signal behavior in different MRI sequences. For instance, fluid mediums appear hypointense in T_1-weighted (T_1w) sequences and hyperintense in T_2-weighted (T_2w) sequences [16]. Sedimented blood, which can be found in hematomas or hemorrhage effusions in body cavities in the living and deceased, can be recognized easily by its typical two-layered morphological appearance [17]. If blood is not sedimented in the deceased, which occurs in the minority of cases, it is harder to discriminate it from other fluids such as serous fluids or bile in conventional MR images [17, 18]. The image reader may still be able to discern different fluid types, such as proteinaceous fluids and hemorrhages by different signal intensities in conventional images [19, 20]. This approach, however, is not always reliable. One approach to discern fluid types and blood reliably may be the use of a recently implemented quantitative MRI sequence. This particular sequence simultaneously quantifies the T_1 and T_2 relaxation times and proton density of the imaged tissue, using a multi-slice saturation recovery turbo spin echo sequence with dual-echo acquisition. Based on the measured T_1, T_2, and proton density (PD) values, conventional T_1-weighted, T_2-weighted, and PD images can be synthesized with a free choice of echo time (TE), repetition time (TR), and inversion time (TI). Synthetic MRI images are similar to conventional MR images, hence allowing the user to work with MRI images normally. The advantage of this technique, however, is that quantitative measurements can be obtained from the same dataset, where all images are intrinsically co-registrated. The quantified parameters T_1 (in ms), T_2 (in ms), and PD (in %, where 100 % is equivalent to pure water) can be used to characterize fluids in an objective manner by measuring and comparing the three different parameters [21–24]. The purpose of the present study was to investigate whether serous fluids, blood, cerebrospinal fluid (CSF), and putrefied CSF can be differentiated and characterized based on their quantitative T_1, T_2, and PD values.

Materials and methods

Study subjects

Blood, serous fluids, CSF, and putrefied CSF from 86 forensic corpses (mean age 51±17.7 years, 44 males, 42 females) were analyzed in a prospective study. The inclusion criteria were as follows: corpses with collections of fluids within the lateral brain ventricles, the thoracic cavities, and abdominal cavities as well as the pericardial sac and the left and right heart ventricles. Blood, serous fluids, and CSF were assessed only in fresh corpses with a postmortem interval (PMI) of 1 to 4 days (time between death and MRI scan). Putrefied CSF was assessed in putrefied corpses. Putrefaction was determined when there were relevant external signs (brown- to green-colored skin veins, ablation of external skin layers, and vesicle formations of the skin) and internal signs of putrefaction. The internal state of decomposition was determined with the radiological alteration index (RAI) from Egger et al. using whole-body computed tomography prior to PMMRI. Only putrefied corpses with a RAI over 60 were included in this study [25, 26]. The PMI of the putrefied corpses ranged from 3 weeks to 3.5 months.

MRI, temperature monitoring, and image analysis

For MRI scanning (Siemens Magnetom Symphony Tim 1.5 T), the corpses were wrapped in an artifact-free body bag or a linen sheet. All subjects were scanned in supine position. The MRI quantification sequence was a multi-slice turbo spin echo (TSE) sequence, where each acquisition was performed with two different echo-times, at 20 and 95 ms. Four different saturation delays times were acquired, at 100, 400, 1100, and 2400 ms, using a TR of 2500 ms. The scan time was 15 min for each brain or heart. In this setup, eight different images were acquired, with different effects of T_1 and T_2 relaxation. The T_1 and T_2 relaxation, as well as proton density (PD), was retrieved by a commercially available post-processing tool (SyMRI Autopsy, SyntheticMR, Linköping, Sweden) [27]. The same software provided the synthetic T_1-weighted, T_2-weighted, and PD images for visual support. Twenty to 24 cardiac short axis slices or brain slices of 4 mm in thickness were acquired with a gap of 0.3 mm. The use of the image data for the present study was approved by the local ethics committee.

During the MRI scan, the corpse temperature was assessed in real time with MR-compatible temperature probes that were placed in the esophagus. The temperatures of the fresh corpses ranged from 4–33 °C (mean temperature 19.3 °C, SD 6.9), and the temperature of the putrefied corpses ranged from 16–21 °C (mean temperature 22.7 °C, SD 4.8).

To obtain quantitative values of fluids, a total of five independent and non-overlapping square regions of interest (ROIs) were placed in three different slices of cardiac short axis MRI images or axial brain MRI images (Fig. 1) by one observer experienced in forensic imaging. The ROIs were placed over the entire ventro-dorsal expansion of the fluid collections. The sizes of the ROIs depended on the extensions of the fluid collections but were at least 0.5 cm in each square dimension. In cases of visible segmentation, the upper and lower layers were measured separately.

The quantitative T_1, T_2, and PD values of serous fluids, blood, and CSF were 3D plotted and related to the body core temperature of the corpse at the time of data acquisition. Because of the low temperature range (16–21 °C) of the putrefied corpses, the putrefied CSF was not related to the body core temperature.

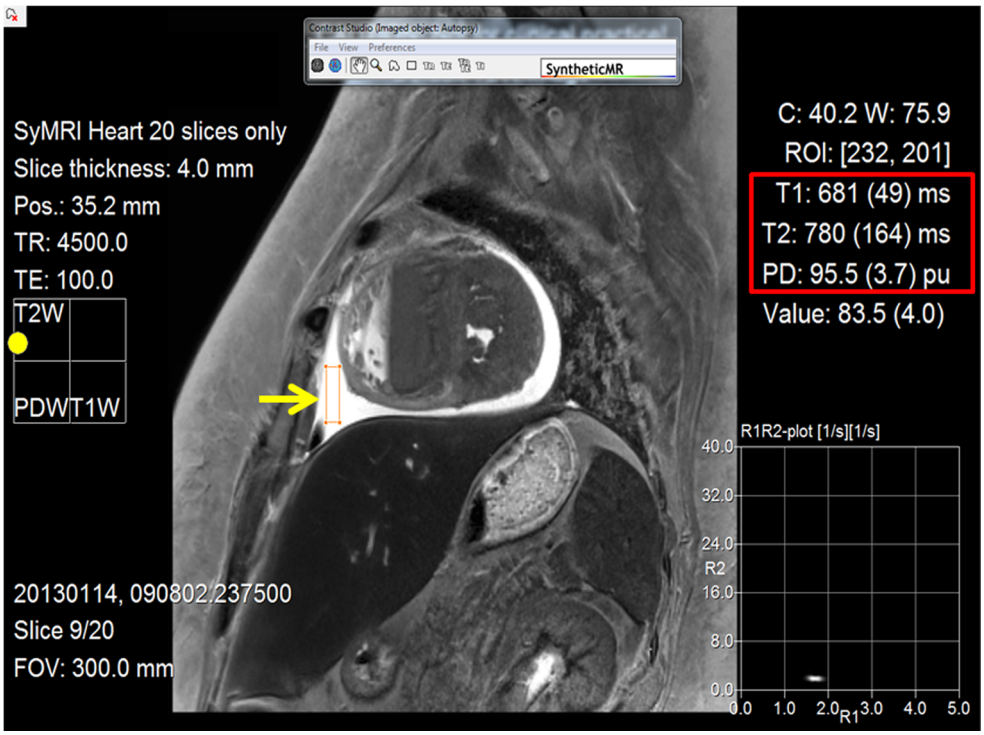

Fig. 1 Synthetically quantified cardiac short axis T_2w MRI image. Quantitative values (*red frame upper right corner*) were obtained by placing ROIs (*yellow arrow*, example measurement shown for a serous fluid collection in the pericardial sac) on detected fluid collections

The ThreeDify Excel Grapher Add-in for Microsoft Excel® was applied to visualize clustering and separation of blood, serous fluids, CSF, and putrefied CSF in 3D plots.

Macroscopic analysis of sampled fluids

Autopsies were authorized by the local authorities and performed by forensic pathologists immediately after MRI scanning or on the following day. The fluid mediums that were measured in the MRI images were obtained at autopsy, and their macroscopic appearance (viscosity, color, and clarity) was examined immediately afterwards. Low viscosity fluids that were light yellow to light red in color and clear or slightly unclear in appearance were characterized as serous fluids in the thoraco-abdominal compartments or CSF in the lateral brain ventricles, respectively. Blood was characterized by its typical red appearance and viscosity. Blood clots were characterized as being compact or thickened blood formations of a red to yellowish color within the right and left heart ventricles. Only blood clots from the heart ventricles were assessed for this study. The lower cellular layers of sedimented blood formations were not considered blood clots. Fluids in the ventricles of putrefied corpses that were dark red to black in color and unclear in appearance were characterized as putrefied CSF. In 7 cases of the 15 putrefied corpses, the macroscopic evaluation of the fluids in the lateral ventricles was not possible because of the highly softened or liquefied consistency of the brain tissues.

At autopsy, fluid mediums were obtained from the following body cavities: serous fluids from the thoracic cavities (n=12) and the pericardial sac (n=13); fluid blood from the right heart and left heart ventricles (n=12), sedimented blood from the pericardial sac (n=2), thoracic cavities (n=6), abdominal cavity (n=2), and left and right heart ventricles (n=18); blood clots from the right and left heart ventricles (n=13); CSF from the lateral brain ventricles (n=16); and putrefied CSF from the lateral brain ventricles (n=15).

Generation of equations for temperature correction and statistical analysis

Using Microsoft Excel®, linear equations were generated to assess the T_1/temperature, T_2/temperature, and PD/temperature relationships for each investigated fluid medium and blood clots. Those equations were used to correct the values of T_1, T_2, and PD: the according corpse temperatures were subtracted from 37 °C (Δ temperatures). Δ temperatures were applied in the equations generated from the quantitative values/temperature relation graphs to gain ΔT_1, ΔT_2, and ΔPD. Those Δ values were summated to the uncorrected T_1, T_2, and PD values to gain the temperature corrected values. Temperature corrections were conducted for serous fluids, blood, blood clots and CSF to a temperature of 37 °C. Due to the small body temperature ranges of the putrefied corpses, no equations for putrefied CSF were generated. Thus, no temperature corrections for the quantitative T_1, T_2, and PD values of putrefied CSF were conducted.

SPSS® was used to analyze quantitative sample data of T_1, T_2, and PD values. The samples were tested for normality using the Kolmogorov-Smirnov test and the Shapiro-Wilk

test. Both tests showed multiple samples that were not normally distributed. Paired Kruskal-Wallis tests were performed to determine significant differences between the samples. Bonferroni's correction was performed to evaluate significant differentiability of quantitative T_1, T_2, and PD values between serous fluids, fluid blood, sedimented blood, blood clots, CSF, and putrefied CSF.

Using the MATLAB® software, the receiver operator characteristic (ROC) curve approach was applied to give accuracy of discrimination between the tested fluids. Accuracy was measured by the area under the ROC curve (AUC) with the traditional academic point system: 0.90–1=excellent; .80–0.90=good; .70–0.80=fair; 0.60–0.70=poor; 0.50–0.60=fail.

Results

Quantitative values/temperature relations

The quantitative values/temperature relations obtained in the investigated cases were expressed by linear equations. Table 1 lists the linear equations generated for serous fluids, fluid blood, sedimented blood, blood clots, and CSF. Individual variations in the relationship between the change in temperature and the change in quantitative values were observed in all investigated mediums. A temperature dependence was observed mainly for the T_1 and the T_2 values of fluid mediums as shown in the example of the plasma layer of sedimented blood in Fig. 2. In the mediums that mainly consisted of red blood cells (blood clots and the erythrocyte layer of sedimented blood), T_2 values did not exhibit a relevant temperature dependence. The PD values were only minimally influenced by temperature in all investigated mediums. Temperature correction to a temperature of 37 °C resulted in lower standard deviations in all investigated mediums.

Differentiation of blood, serous fluids, CSF, and putrefied CSF with quantitative values

Table 2 shows the mean quantitative values (T_1 and T_2 relaxation times as well as PD) obtained for serous fluids, fluid blood, sedimented blood, blood clots, CSF, and putrefied CSF in 86 forensic cases. All fluid mediums except the putrefied CSF (n=15) were correlated with body temperature at the time of MRI scanning. Statistical analysis revealed that temperature correction had no significant influence on the differentiability of all investigated fluids. Quantitative values were plotted in a 3D-coordinate system and are depicted with and without correction for a temperature of 37 °C (Fig. 3). In the 3D plot as well as in statistical analysis, the quantitative values of serous fluids and CSF could be well discriminated from the values of fluid blood, sedimented blood and blood clots. Putrefied CSF could be differentiated from all other investigated fluid mediums. The quantitative values of the serous fluids in the pericardial sac clearly differed from those of the serous fluids in the thoracic cavities in the 3D plot. The quantitative values of fluid blood, sedimented blood, and blood clots were all distinguishable from each other in the 3D plot as well as in statistical analysis. Furthermore, the investigated blood fractions differed significantly from blood clots (Fig. 3 and Table 3).

Discussion

In the present postmortem study, the synthetic MRI approach was applied for the first time to investigate different fluids within the body. Serous fluids, fluid blood, sedimented blood, blood clots, CSF, and putrefied CSF could be well differentiated from each other by their quantitative values of T_1, T_2, and PD. This provides the basis for further promising applications of quantitative MRI. Databases for quantitative values of T_1, T_2, and PD of fluids can be established. As a result, a scale of quantitative values for fluids can be created similar to the Hounsfield scale in CT applications. Using quantitative data from synthetic MRI applications also provides the basis for automatic fluid detection and computer-aided diagnosis. Synthetic MRI images can be loaded on a personal computer with properly adapted software. Then, computer-aided diagnostics can be implemented based on established values of the signal behavior of the fluid mediums [28–30]. For example, blood could automatically be detected and encoded in color. This could help the image reader detect hemorrhages and

Table 1 Linear equations for fluids and blood clots generated from the relation of T_1, T_2, and PD to body core temperature at the time of scanning as obtained from 71 forensic cases

	Fluid blood	Blood plasma layer	Erythrocyte layer	Blood clot	Serous fluids	CSF
T_1/temperature	T_1=6.63x+507	T_1=4.93x+562	T_1=7.8x+449	T_1=4.63x+454	T_1=3.9x+819	T_1=4.65x+585
T_2/temperature	T_2=7.42x+159	T_2=8.93x+239	T_2=−1.05x+79	T_2=1.69x+70	T_2=23.01x+479	T_2=32.27x+418
PD/temperature	PD=0.43x+74	PD=0.44x+82	PD=0.43x+68	PD=0.44x+66	PD=−0.59x+101	PD=0.19x+82

Due to small temperature ranges, no equations for putrefied CSF were generated. (T_1: T_1 relaxation time in milliseconds; T_2: T_2 relaxation time in milliseconds; T: body core temperature in °C; PD: PD in % related to pure water (100 %))

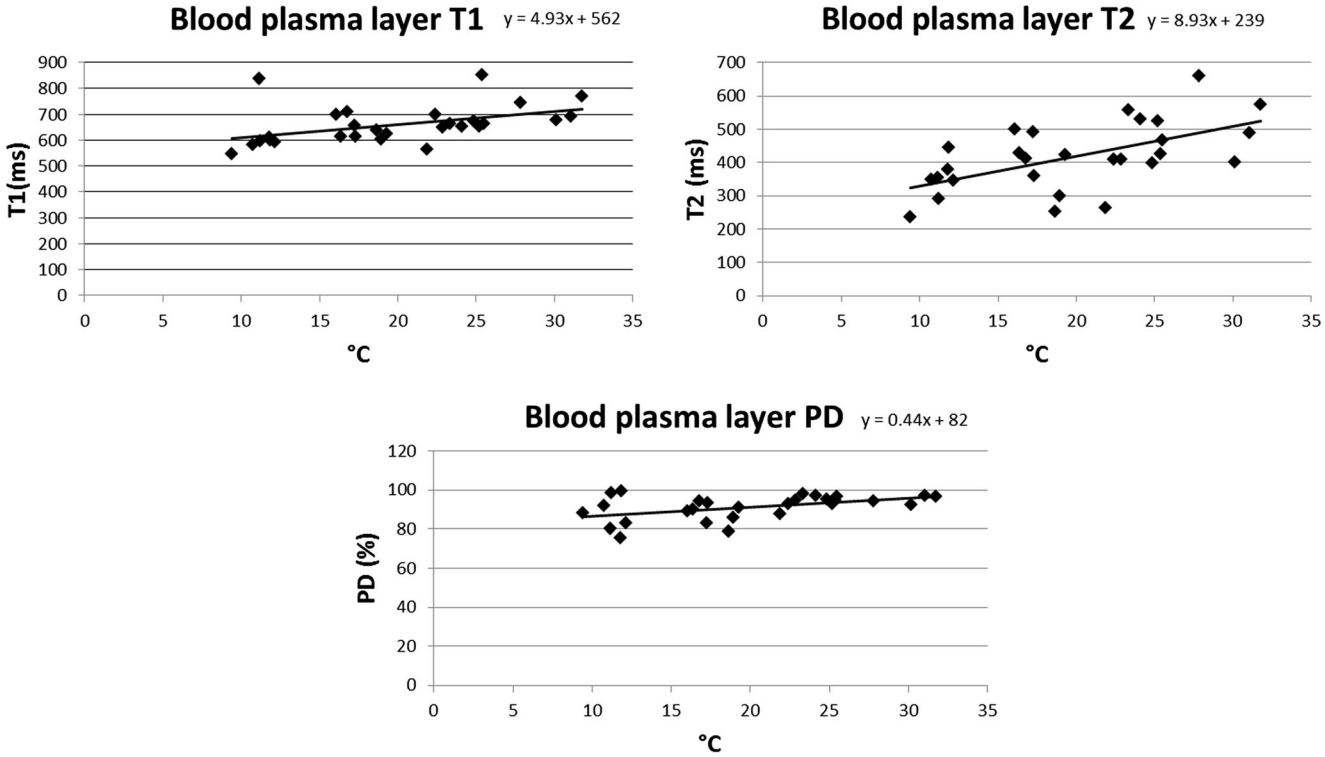

Fig. 2 Sample plots of the T_1 and T_2 relaxation times and PD of the plasma layer of sedimented blood vs. body core temperature at the time of scanning. Note that there is a temperature dependence mainly for the T_1 and T_2 values. It was assumed that the quantitative T_1, T_2, and PD values correlate linearly with rising temperature. Linear equations for temperature correction are depicted on the *upper right corner* of each table

discriminate blood from other fluid mediums in the corpse. The detection of blood collections may also be relevant in the decision to perform postmortem CT-angiography to detect the source of exsanguination [31, 32].

The temperature dependence of the quantitative values challenges the postmortem synthetic MRI approach. In the present study, this temperature dependence was observed mainly for the T_1 and T_2 relaxation times in serous fluids, blood, and blood clots. Preliminary studies demonstrated a temperature dependence of T_1 relaxation times in blood. It was shown that the T_1 relaxation time correlated with rising temperature [33–39]. Our data confirmed a correlation between the T_1 values and rising temperature. A new finding we observed was a relevant T_2 temperature dependence for fluids as well. In forensic practice, corpses are scanned with temperatures usually ranging between 0 and 40 °C. To compare quantitative MRI data from different corpse scans, the temperature dependence of the quantitative values has to be taken into account. A valid comparison of different MRI scans is possible only when the quantitative values gained from the scans are corrected for temperature. Then, the temperature-caused differences between individual corpses can be

Table 2 Mean quantification values (T_1 and T_2 in ms; PD in %) and 95 % confidence intervals (CI) of the investigated fluids and blood clots obtained from 5 measurements in 86 forensic cases

	T_1 uncorrected (CI)	T_1 corrected to 37 °C (CI)	T_2 uncorrrected (CI)	T_2 corrected to 37 °C (CI)	PD uncorrected (CI)	PD corrected to 37 °C (CI)
Fluid blood	659 (18)	805 (19)	492 (12)	472 (11)	82 (3)	90 (4)
Blood plasma layer	660 (27)	744 (24)	417 (29)	570 (31)	91 (6; 2)	99 (2)
Erythrocyte layer	608 (27)	742 (19)	57 (6)	39 (5)	76 (2)	84 (2)
Blood clot	538 (26)	625 (19)	101 (12)	133 (11)	74 (3)	82 (3)
Serous fluids	752 (41)	746 (47)	850 (124)	1293 (107)	92 (3)	81 (6)
CSF	695 (43)	757 (22)	1052 (151)	1612 (27)	86 (5)	89 (5)
Putrefied CSF	578 (22)	–	231 (17)	–	92 (4)	–

Data are presented with (except for putrefied CSF) and without correction to 37 °C

equalized. In the present study, linear equations to correct for the temperature dependence of T_1, T_2, and PD quantitative values of fluid mediums to 37 °C were introduced. The correction of quantitative values to 37 °C resulted in slightly better discrimination between the fluid mediums in the 3D plot as well as in the statistical analyses, which supports the assertion that temperature correction is needed.

The present study has several limitations. Measurements were taken by only one observer, and no statistical reproducibility analysis of quantitative value measurement was conducted. It is likely to expect that there would be a variability of quantitative values between different observers. However, the conducted measurement technique is relatively easy to perform and the results of the present study rather do not indicate that the expected inter observer variability would have relevant influence on the differentiability of fluids. Furthermore for some fluids, only small numbers could be assessed. To create databases with regular quantitative T_1, T_2, and PD values for different fluids and blood, a larger number of cases will be required. Additionally, the investigated fluids and blood were not examined histologically or chemically. We observed differences in the quantitative values of serous fluids in the pericardial sac compared with serous fluids in the thoracic cavities and CSF in the lateral brain ventricles. It can be assumed that different protein densities and cellular impurities are responsible for the differing quantitative values in serous fluids and CSF [26, 40–42]. The possibility of detecting changes in cellular components and protein density in serous fluids and CSF based on quantitative values may be of relevant interest because a measurable change in the chemical composition of fluids may be a noninvasive indicator of pathologic conditions such as inflammation or tumors. It is noteworthy that quantitative MRI is not the only promising approach to discern various fluid types. Clinical studies showed that it is possible to differentiate serous and purulent infectious fluids by means of diffusion-weighted MRI [43, 44]. Other approaches such as the application of magnetization transfer ratio and NMR spectroscopy are also potentially feasible to discriminate different fluids types [45–48].

Interestingly, we were able to observe that differentiation between the cellular layers of sedimented blood and blood clots was possible based on their quantitative values. This may be explained by different contents of proteins in the coagulation cascade, activation of platelets and platelet factors, and arrangement of cellular components within the cellular layer of sedimented blood compared with blood clots. If quantitative MRI is feasible for detecting different protein contents in mediums consisting mainly of blood cells, it might also be used to differentiate between vital thrombi and postmortem blood clots. So far, the gold standard for recognizing a vital thrombus is histologic diagnosis based on the layered arrangement of cellular components and the existence of cross-linked fibrin meshes [42, 49]. Jackowski et al. demonstrated that conventional unenhanced 3-T MRI is also feasible for detecting pulmonary thromboembolism via the changes in signal intensity of thrombi in conventional MRI images [50]. However, diagnosis of pulmonary thromboembolism in conventional MRI images is always challenging and often inconclusive. Further investigations that compare quantitative values of vital thrombi and postmortem blood clots are necessary.

Fig. 3 Three defined views (PD/T_1 view, T_2/T_1 view, and PD/T_2 view) on a 3D plot of fluids and blood clots based on T_1 and T_2 relaxation times and PD. Values are depicted as not corrected for temperature (**a**) and corrected for a temperature of 37 °C (**b**). The serous fluids from the thoracic cavities and pericardial sac are depicted with *different colors*. Note that the clusters of CSF and serous fluids on the one hand and fluid blood and sedimented blood on the other hand can be well differentiated from each other. The depicted values corrected for a temperature of 37 °C allow for better discrimination between the single fluids, which can be seen best in the T_1/T_2 and PD/T_2 views. Putrefied CSF can be differentiated from all other investigated fluids in the plots that were not corrected for temperature (due to small temperature ranges, putrefied CSF was not corrected for temperature)

For the first time, quantitative values of putrefied fluids were evaluated. Based on their quantitative values, the investigated putrefied fluids in the lateral brain ventricles could be clearly differentiated from the CSF in the lateral brain ventricles as well as from all other investigated fluids of fresh corpses. However, the quantitative values of putrefied thoraco-abdominal fluids were not assessed. It may be possible that these values differ from the putrefied CSF values due to differing tissue compositions of thoraco-abdominal organs and fluids [42]. If the quantitative values of putrefied fluids are known entirely, they may be used to discriminate the fluids from relevant forensic ante mortem pathologies. The results of the present study indicate that, for example, antemortem hemorrhages in putrefied corpses could be detected and characterized based on their quantitative values. Further investigations and assessment of putrefied brain tissues as well as of putrefied thoraco-abdominal organs, fluids, and pathologies are necessary.

A 1.5-T MR scanner was used for the present study. Because the relaxation times depend on the strength of the magnetic field, it is reasonable to expect that the use of MR scanners with different magnetic field strengths, such as 3 T, will result in different quantitative values for T_1 and T_2 for the same fluids and temperatures [16]. Therefore, it is inevitable that the quantitative values of the relaxation times of fluids have to be adapted not only to different temperatures but also to different magnetic field strengths.

Conclusions

Postmortem 1.5-T MR quantification using a combination of the relaxation times of T_1 and T_2 and the PD value allows for reliable discrimination and characterization of serous fluids,

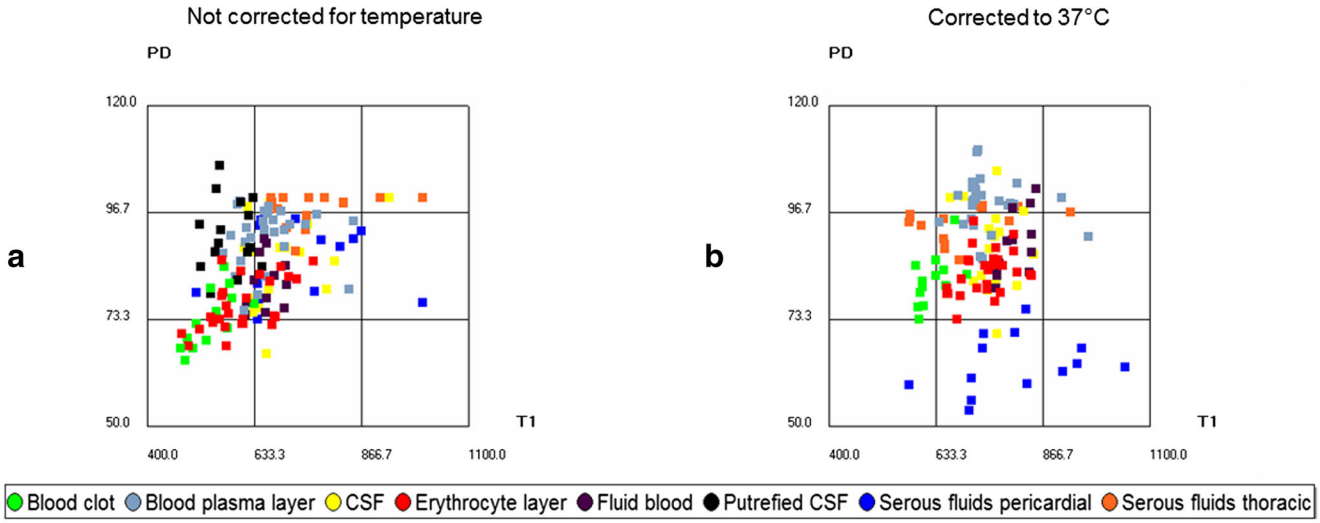
Not corrected for temperature
Corrected to 37°C
PD
T1
a
b
120.0
96.7
73.3
50.0
400.0
633.3
866.7
1100.0
Blood clot
Blood plasma layer
CSF
Erythrocyte layer
Fluid blood
Putrefied CSF
Serous fluids pericardial
Serous fluids thoracic

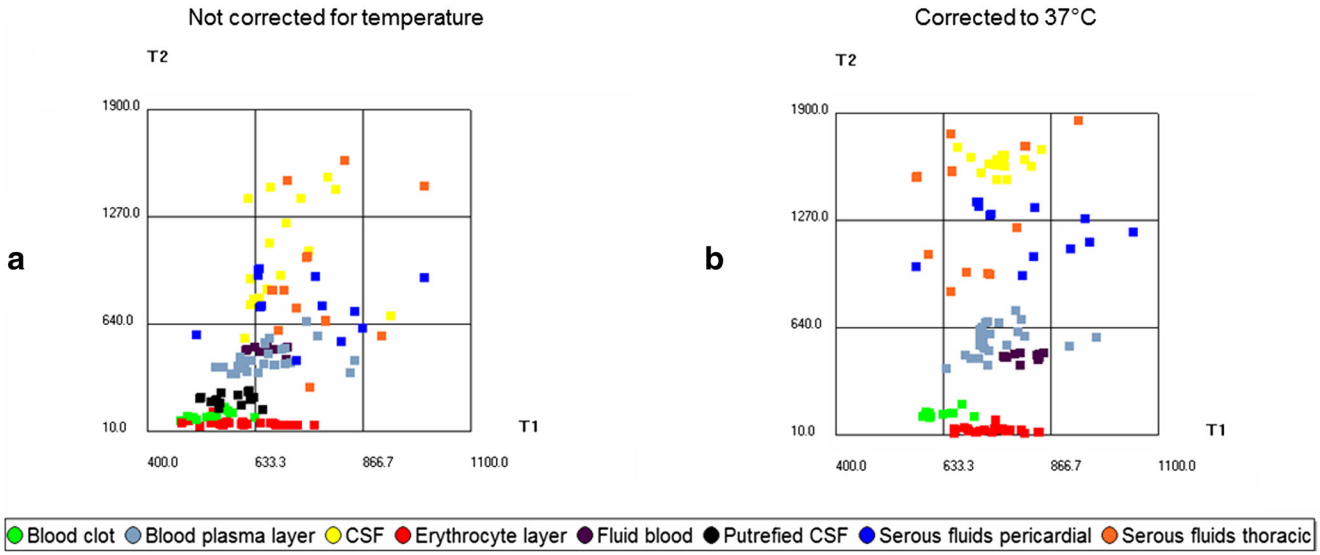
Not corrected for temperature
Corrected to 37°C
T2
T1
a
b
1900.0
1270.0
640.0
10.0
400.0
633.3
866.7
1100.0
Blood clot
Blood plasma layer
CSF
Erythrocyte layer
Fluid blood
Putrefied CSF
Serous fluids pericardial
Serous fluids thoracic

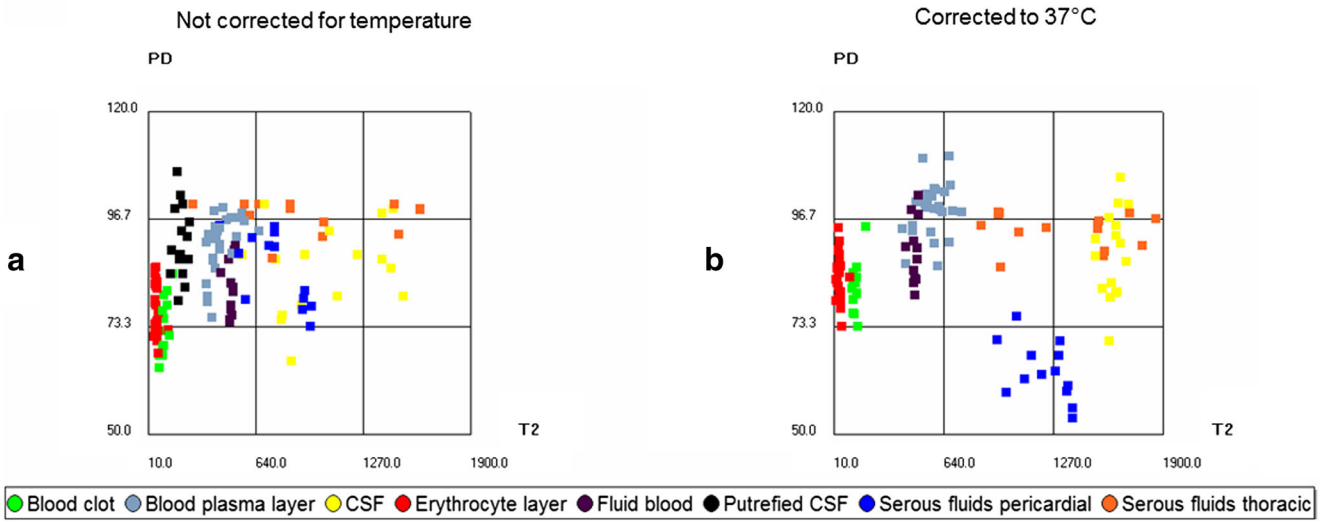
Not corrected for temperature
Corrected to 37°C
PD
T2
a
b
120.0
96.7
73.3
50.0
10.0
640.0
1270.0
1900.0
Blood clot
Blood plasma layer
CSF
Erythrocyte layer
Fluid blood
Putrefied CSF
Serous fluids pericardial
Serous fluids thoracic

Table 3 Results of the Kruskal-Wallis tests for comparison of quantitative values for T_1 (ms), T_2 (ms), and PD (%) between serous fluids, fluid blood, sedimented blood, blood clots, CSF, and putrefied CSF in 86 forensic cases

	Significance			ROC-AUC/accuracy not corrected	Significance			ROC-AUC/accuracy corrected to 37 °C	
	T_1 not corrected	T_2 not corrected	PD not corrected		T_1 corrected to 37 °C	T_2 corrected to 37 °C	PD corrected to 37 °C		
Fluid blood-blood plasma layer	0.526	0.01	*<0.001*	0.95/excellent	*0.001*	*<0.001*	*0.001*	0.96/excellent	Fluid blood-blood plasma layer
Fluid blood-erythrocyte layer	0.025	*<0.001*	0.01	1/excellent	*0.001*	*<0.001*	0.014	1/excellent	Fluid blood-erythrocyte layer
Fluid blood-blood clot	*<0.001*	*<0.001*	0.007	1/excellent	*<0.001*	*<0.001*	0.006	1/excellent	Fluid blood-blood clot
Fluid blood-serous fluids	0.003	*<0.001*	*0.001*	1/excellent	0.034	*<0.001*	*0.001*	1/excellent	Fluid blood-serous fluids
Erythrocyte layer-blood clot	0.005	*<0.001*	0.161	0.96/excellent	*<0.001*	*<0.001*	0.132	1/excellent	Erythrocyte layer-blood clot
Erythrocyte layer-blood plasma layer	0.017	*<0.001*	*<0.001*	1/excellent	0.623	*<0.001*	*<0.001*	1/excellent	Erythrocyte layer-blood plasma layer
Erythrocyte layer-serous fluids	*<.0.001*	*<0.001*	*<0.001*	1/excellent	*<0.001*	*<0.001*	*<0.001*	1/excellent	Erythrocyte layer-serous fluids
Blood plasma layer-blood clot	*<0.001*	*<0.001*	*<0.001*	1/excellent	*<0.001*	*<0.001*	*<0.001*	1/excellent	Blood plasma layer-blood clot
Blood plasma layer-serous fluids	*0.001*	*<0.001*	0.148	1/excellent	0.886	*<0.001*	*<0.001*	1/excellent	Blood plasma layer-serous fluids
Serous fluids-blood clot	*<.0.001*	*<0.001*	*<0.001*	1/excellent	*<0.001*	*<0.001*	*<0.001*	1/excellent	Serous fluids-blood clot
CSF-fluid blood	0.458	*<0.001*	0.185	1/excellent	*0.003*	*<0.001*	*0.089*	1/excellent	CSF-fluid blood
CSF-blood plasma layer	0.140	*<0.001*	0.060	1/excellent	0.075	*<0.001*	*0.001*	1/excellent	CSF-blood plasma layer
CSF-erythrocyte layer	*0.002*	*<0.001*	*<0.001*	1/excellent	0.294	*<0.001*	*<0.001*	1/excellent	CSF-erythrocyte layer
CSF-blood clot	*<0.001*	*<0.001*	0.031	1/excellent	*<0.001*	*<0.001*	0.025	1/excellent	CSF-blood clot
CSF-serous fluids	0.034	0.044	0.031	0.82/good	0.029	*<0.001*	0.0026	0.85/good	CSF-serous fluids
Putrefied CSF-CSF	*<0.001*	*<0.001*	0.113	1/excellent	–	–	–	–	Putrefied CSF-CSF
Putrefied CSF-fluid blood	*<0.001*	*<0.001*	0.003	1/excellent	–	–	–	–	Putrefied CSF-fluid blood
Putrefied CSF-blood plasma layer	*<0.001*	*<0.001*	0.970	1/excellent	–	–	–	–	Putrefied CSF-blood plasma layer
Putrefied CSF-erythrocyte layer	0.146	*<0.001*	*<0.001*	1/excellent	–	–	–	–	Putrefied CSF-erythrocyte layer
Putrefied CSF-blood clot	0.050	*<0.001*	*<0.001*	1/excellent	–	–	–	–	Putrefied CSF-blood clot
Putrefied CSF-serous fluids	*<0.001*	*<0.001*	0.542	1/excellent	–	–	–	–	Putrefied CSF-serous fluids

Tests were performed separately between T_1, T_2, and PD variables. Significance results are given with (except for putrefied CSF) and without correction to 37 °C. Bonferroni correction was applied: for not corrected values: asymptotic significance <0.0033; for corrected values: asymptotic significance <0.0023. Significant differences between the samples are highlighted in italicized numbers. A significant difference between all tested fluid mediums can be determined. The table also gives the area under the ROC curve (ROC/AUC) for the tested fluids and mediums (not corrected and corrected to 37 °C). Except for one group (CSF-serous fluids) accuracy of discrimination was excellent in all tested groups

fluid blood, sedimented blood, blood clots, CSF, and putrefied CSF. The quantification approach allows for computer-aided detection and diagnosis of hemorrhages. The quantitative values of mainly T_1 and T_2 were temperature dependent. Equations to correct for the temperature dependence at 1.5 T have been introduced.

Acknowledgments The authors would like to thank the team of forensic pathologists and forensic autopsy technicians at the Institute of Forensic Medicine Bern for their support in handling the cases.

References

1. Lundström C, Persson A, Ross S et al (2012) State-of-the-art of visualization in post-mortem imaging. APMIS 120:316–326
2. Jackowski C, Schwendener N, Grabherr S, Persson A (2013) Postmortem cardiac 3T magnetic resonance imaging: visualizing the sudden cardiac death? J Am Coll Cardiol 62(7):617–629
3. Roberts IS, Benbow EW, Bisset R et al (2003) Accuracy of magnetic resonance imaging in determining cause of sudden death in adults: comparison with conventional autopsy. Histopathology 42: 424–430
4. Thali MJ, Yen K, Schweitzer W et al (2003) Virtopsy, a new imaging horizon in forensic pathology: virtual autopsy by postmortem multislice computed tomography (MSCT) and magnetic resonance imaging (MRI)—a feasibility study. J Forensic Sci 48(2):386–403
5. Dirnhofer R, Jackowski C, Vock P, Potter K, Thali MJ (2006) VIRTOPSY: minimally invasive, imaging-guided virtual autopsy. Radiographics 26(5):1305–1333
6. Patriquin L, Kassarjian A, Barish M et al (2001) Postmortem whole-body magnetic resonance imaging as an adjunct to autopsy: preliminary clinical experience. J Magn Reson Imaging 13:277–287
7. Brogdon BG (2010) Brogdon's forensic radiology, 2nd edn. CRC Press, Boca Raton
8. Aghayev E, Christe A, Sonnenschein M, Yen K, Jackowski C, Thali MJ, Dirnhofer R, Vock P (2008) Postmortem imaging of blunt chest trauma using CT and MRI: comparison with autopsy. J Thorac Imaging 23(1):20–27
9. Bolliger SA, Thali MJ, Aghayev E, Jackowski C, Vock P, Dirnhofer R, Christe A (2007) Postmortem noninvasive virtual autopsy: extrapleural hemorrhage after blunt thoracic trauma. Am J Forensic Med Pathol 28(1):44–47
10. Aghayev E, Sonnenschein M, Jackowski C et al (2006) Postmortem radiology of fatal hemorrhage: measurements of cross-sectional areas of major blood vessels and volumes of aorta and spleen on MDCT and volumes of heart chambers on MRI. AJR 187:209–215
11. Montano-Loza AJ (2013) New concepts in liver cirrhosis: clinical significance of sarcopenia in cirrhotic patients. Minerva Gastroenterol Dietol 59(2):173–186
12. Treglia G, Sadeghi R, Annunziata S, Lococo F, Cafarotti S, Bertagna F, Prior JO, Ceriani L, Giovanella L (2014) Diagnostic accuracy of (18)F-FDG-PET and PET/CT in the differential diagnosis between malignant and benign pleural lesions: a systematic review and meta-analysis. Acad Radiol 21(1):11–20
13. Solooki M, Miri M (2013) Approach to undiagnosed exudative pleural effusion: the diagnostic yield of blind pleural biopsy. Caspian J Intern Med 4(2):642–647
14. Huang XE, Wei GL, Huo JG, Wang XN, Lu YY, Wu XY, Liu J, Xiang J, Feng JF (2013) Intrapleural or intraperitoneal lobaplatin for treatment of patients with malignant pleural effusion or ascites. Asian Pac J Cancer Prev 14(4):2611–2614
15. Adhikari P, Pathak UN, Uprety D, Sapkota S (2012) Profile of ascites patient admitted in Nepal Medical College Teaching Hospital. Nepal Med Coll J 14(2):111–113
16. Haacke ME, Brown RW, Thompson MR, Venkatesh N (1999) Magnetic resonance imagingphysical principles and sequence design. Wiley, New York
17. Jackowski C, Thali M, Aghayev E, Yen K, Sonnenschein M, Zwygart K, Dirnhofer R, Vock P (2006) Postmortem imaging of blood and its characteristics using MSCT and MRI. Int J Legal Med 120(4):233–240
18. Schleyer F (1958) Postmortem blood viscosity, blood cell volume, osmotic erythrocyte resistance and blood sedimentation in relation to cadaver age and cause of death. Virchows Arch 331(3):276–286
19. Shiono T, Yoshikawa K, Takenaka E, Hisamatsu K (1993) MR imaging of pleural and peritoneal effusion. Radiat Med 11(4): 123–126
20. Aprile I, Iaiza F, Lavaroni A, Budai R, Dolso P, Scott CA, Beltrami CA, Fabris G (1999) Analysis of cystic intracranial lesions performed with fluid-attenuated inversion recovery MR imaging. AJNR Am J Neuroradiol 20(7):1259–1267
21. Warntjes JB, Dahlqvist O, Lundberg P (2007) Novel method for rapid, simultaneous T1, T*2, and proton density quantification. Magn Reson Med 57:528–537
22. Warntjes JB, Leinhard OD, West J, Lundberg P (2008) Rapid magnetic resonance quantification on the brain: optimization for clinical usage. Magn Reson Med 60:320–329
23. Warntjes MJ, Kihlberg J, Engvall J (2010) Rapid T1 quantification based on 3D phase sensitive inversion recovery. BMC Med Imaging 10:19
24. Blystad I, Warntjes JB, Smedby O, Landtblom AM, Lundberg P, Larsson EM (2012) Synthetic MRI of the brain in a clinical setting. Acta Radiol 53:1158–1163
25. Egger C, Vaucher P, Doenz F, Palmiere C, Mangin P, Grabherr S (2012) Development and validation of a postmortem radiological alteration index: the RA-Index. Int J Legal Med 126(4):559–566
26. Zech WD, Jackowski C, Buetikofer Y, Kara L (2014) Characterization and differentiation of body fluids, putrefaction fluid, and blood using Hounsfield unit in postmortem CT. Int J Legal Med 128(5):795–802
27. Synthetic MR products website. Available at: http://www.syntheticmr.com. Accessed 30 June 2014
28. Ljung P, Winskog C, Persson A, Lundström C, Ynnerman A (2006) Full body virtual autopsies using a state-of-the-art volume rendering pipeline. IEEE Trans Vis Comput Graph 12:869–876
29. Jackowski C, Warntjes MJ, Kihlberg J, Berge J, Thali MJ, Persson A (2011) Quantitative MRI in isotropic spatial resolution for forensic soft tissue documentation. Why and how ? J Forensic Sci 56: 208–215
30. Persson A, Lindblom M, Jackowski C (2011) A state-of-the-art pipeline for postmortem CT and MRI visualization: from data acquisition to interactive image interpretation at autopsy. Acta Radiol 52:522–536
31. Grabherr S, Grimm J, Dominguez A, Vanhaebost J, Mangin P (2014) Advances in postmortem CT-angiography. Br J Radiol 87(1036):20130488
32. Jackowski C, Persson A, Thali MJ (2008) Whole body postmortem angiography with a high viscosity contrast agent solution using poly ethylene glycol as contrast agent dissolver. J Forensic Sci 53(2):465–468
33. Dickinson RJ, Hall AS, Hind AJ, Young IR (1986) Measurement of changes in tissue temperature using MR imaging. J Comput Assist Tomogr 10:468–472
34. Wlodarczyk W, Hentschel M, Wust P et al (1999) Comparison of four magnetic resonance methods for mapping small temperature changes. Phys Med Biol 44:607–624

35. Peller M, Kurze V, Loeffler R et al (2003) Hyperthermia induces T1 relaxation and blood flow changes in tumors. A MRI thermometry study in vivo. Magn Reson Imaging 21:545–551
36. Parker DL, Smith V, Sheldon P, Crooks LE, Fussell L (1983) Temperature distribution measurements in two-dimensional NMR imaging. Med Phys 10:321–325
37. Bertsch F, Mattner J, Stehling MK et al (1998) Non-invasive temperature mapping using MRI: comparison of two methods based on chemical shift and T1-relaxation. Magn Reson Imaging 16:393–404
38. Youl BD, Hawkins CP, Morris JK, DuBoulay EP, Tofts PS (1992) In vivo T1 values from guinea pig brain depend on body temperature. Magn Reson Med 24:170–173
39. Ruder TD, Hatch GM, Siegenthaler L et al (2012) The influence of body temperature on image contrast in post mortem MRI. Eur J Radiol 81:1366–1370
40. Block DR, Algeciras-Schimnich A (2013) Body fluid analysis: clinical utility and applicability of published studies to guide interpretation of today's laboratory testing in serous fluids. Crit Rev Clin Lab Sci 50(4-5):107–124
41. Bonnema J, Ligtenstein DA, Wiggers T, van Geel AN (1999) The composition of serous fluid after axillary dissection. Eur J Surg 165(1):9–13
42. Brinkmann B, Madea B (2004) Handbuch gerichtliche Medizin, vol 1, 1st edn. Springer, Berlin
43. Spüntrup E, Bücker A, Adam G, van Vaals JJ, Günther RW (2001) Differentiation of serous and purulent fluids in vitro and in vivo by means of diffusion-weighted MRI. Röfo 173(1):65–71
44. Gaviani P, Schwartz RB, Hedley-Whyte ET, Ligon KL, Robicsek A, Schaefer P, Henson JW (2005) Diffusion-weighted imaging of fungal cerebral infection. AJNR Am J Neuroradiol 26(5):1115–1121
45. Jia G, Takayama Y, Flanigan DC, Kaeding CC, Zhou J, Chaudhari A, Clark D et al (2011) Quantitative assessment of mobile protein levels in human knee synovial fluid: feasibility of chemical exchange saturation transfer (proteinCEST) MRI of osteoarthritis. Magn Reson Imaging 29(3):335–341
46. Mishra AM, Reddy SJ, Husain M, Behari S, Husain N, Prasad KN, Kumar S, Gupta RK (2006) Comparison of the magnetization transfer ratio and fluid-attenuated inversion recovery imaging signal intensity in differentiation of various cystic intracranial mass lesions and its correlation with biological parameters. J Magn Reson Imaging 24(1):52–56
47. Kumar V, Dwivedi DK, Jagannathan NR (2014) High-resolution NMR spectroscopy of human body fluids and tissues in relation to prostate cancer. NMR Biomed 27(1):80–89
48. Lam CW, Law CY (2014) Pleural effusion lipoproteins measured by NMR spectroscopy for diagnosis of exudative pleural effusions: a novel tool for pore-size estimation. J Proteome Res 13(9):4104–4112
49. Bohm E, Hochkirchen KH (1983) Ultrastructure of intravital, postmortem and autolysed fibrin. Forensic Sci Int 21:117–127
50. Jackowski C, Grabherr S, Schwendener N (2013) Pulmonary thrombembolism as cause of death on unenhanced postmortem 3T MRI. Eur Radiol 23(5):1266–1270